Rapid #: -13100919

CROSS REF ID: **646345**

LENDER: **LHL4CRLRM :: Main Library**

BORROWER: **MFM :: Main Library**

TYPE:	Article CC:CCG
JOURNAL TITLE:	Advances in cement research
USER JOURNAL TITLE:	Advances in Cement Research
ARTICLE TITLE:	Effect of silica fume and fly ash on pore structures of blended pastes at low water to binder ratios
ARTICLE AUTHOR:	
VOLUME:	27
ISSUE:	9
MONTH:	October
YEAR:	2015
PAGES:	506 - 514
ISSN:	0951-7197
OCLC #:	

Processed by RapidX: 4/3/2018 3:28:58 PM

Advances in Cement Research
Volume 27 Issue 8
Effect of silica fume and fly ash on pore structures of blended pastes at low water to binder ratios
Zhao and Sun

ice
Institution of Civil Engineers
publishing

Effect of silica fume and fly ash on pore structures of blended pastes at low water to binder ratios

Sujing Zhao
Jiangsu Key Laboratory of Construction Materials, School of Material Science and Engineering, Southeast University, Nanjing, China

Wei Sun
Jiangsu Key Laboratory of Construction Materials, School of Material Science and Engineering, Southeast University, Nanjing, China

Cementitious materials with very low water to binder (w/b) ratios such as ultra-high-performance concrete (UHPC) have been increasingly used, and their superior performance is largely dependent on the improved pore structures. The benefits of incorporating supplementary cementitious materials (SCMs) to prepare these materials have been widely recognised, whereas there is a lack of research to reveal the effect of SCMs on the pore structure. The aim of this study is to investigate the influence of silica fume and fly ash on the pore structures of blended pastes at such low w/b ratios. Two curing regimes, standard moisture curing and steam curing, were adopted and the pore structures were determined by mercury intrusion porosimetry. The results show that the addition of silica fume refined the pore structure regardless of the curing method and age. The addition of fly ash decreased the porosity after 7 d, whereas the critical pore size was almost unaffected by fly ash under standard curing. Compared to 90 d standard curing, steam curing contributed to a decreased porosity for all the pastes and a reduced critical pore size for the reference and fly ash paste. Moreover, the introduction of both SCMs resulted in a similar pore structure to that of the silica fume paste.

Introduction

With 3 t used annually per person, concrete is the most utilised man-made material in the world. Despite some advantages of concrete such as low cost and high resistance to chemical attack, high volumes of cement production account for 5–8% carbon dioxide emission, which has caused serious deterioration of the ecological environment. Therefore, with the advancement of concrete technology, high-performance concrete (HPC) and ultra-high-performance concrete (UHPC) were developed and have been increasingly used recently. These materials provide attractive workability and remarkable mechanical properties, and more importantly, they exhibit much higher durability than conventional concrete. The extended service life could contribute to a lower life-cycle cost, which promotes sustainability.

The key to make concrete a high-performance one is to lower the water to binder (w/b) ratio, and this became possible with the advent of superplasticiser. To prepare UHPC, the w/b ratio is usually lowered to be less than 0·20 and silica fume is added as a necessary ingredient (Richard and Cheyrezy, 1995). Silica fume is an ultra-fine powder collected as a by-product from silicon and ferrosilicon alloy production, and it can improve the packing density and produce more gel products to make the concrete more compact. Moreover, as a widely used by-product in producing concrete and blended cement, fly ash has also been used as one of the raw materials to produce UHPC (Yazıcı *et al.*, 2009; Zhao *et al.*, 2014). Fly ash cannot play the part of silica fume but can partially substitute cement to constitute a ternary binder system. The addition of fly ash not only brings economic and environmental benefits, but improves the workability and long-term durability (Mehta, 2004; Radlinski and Olek, 2012).

Fundamental properties of cementitious materials, such as strength, shrinkage and durability, are highly dependent on their pore structures. To determine the pore structure, several different methods such as mercury intrusion porosimetry (MIP) (Cook and Hover, 1993), image-based method (Scrivener, 1989), nitrogen sorption/desorption (NSD) (Seaton, 1991) and thermoporometry (TPM) (Sun and Scherer, 2010) have been used. Owing to its limited resolution, an image-based method can only measure large pores. NSD and TPM are both effective methods, but only to measure small pores. The minimum pore sizes detected by NSD and TPM are 2 and 4 nm, respectively, and the upper limit is about 100 nm. Compared to other methods, MIP can measure a wide range of pores and thus is the most commonly adopted technique for determining the pore system in cementitious materials (Atahan *et al.*, 2009; Cook and Hover, 1999; Zeng *et al.*, 2012; Zhou *et al.*, 2010). However, this method has intrinsic limitations owing to the existence of ink-bottle pores (Diamond, 2000; Moro and Böhni, 2002). MIP results in an underestimation

of large pores and an overestimation of small pores; that is, the large pores can only be entered through the small pores and therefore the porosimeter attributes the volume of a large pore to the size of its entrance. Therefore, MIP measurements cannot provide an actual pore size distribution (PSD), but the total porosity and the critical pore width which corresponds to the highest rate of mercury intrusion per change in pressure can still be used as comparative indices to evaluate the capacity and connectivity of pore systems in different samples (Diamond, 2000).

Cementitious materials with very low w/b ratios such as UHPC have been revealed to have a very low porosity as well as a very fine pore structure (Cheyrezy *et al.*, 1995), but few studies have reported on how the addition of supplementary cementitious materials (SCMs) influences the pore structures of such materials. The objective of this study is to investigate the effects of the addition of silica fume and fly ash on the pore structures of cement pastes at very low w/b ratios. The total porosities and critical pore sizes of different samples under varied curing are tested by MIP and the results are discussed.

Materials, mix proportions and sample preparation

Ordinary Portland cement, class F fly ash and silica fume were used as cementitious materials. The physical properties and chemical composition of the cementitious materials are given in Table 1. The specific surface area of the fly ash was higher than that of the cement, which indicates that the mean particle size of the fly ash was smaller compared to that of the cement. Potable tap water and polycarboxylate-based superplasticiser were used.

Four different pastes were designed and their mix proportions are given in Table 2. A naming convention for the pastes was used based on the mix design of each paste. C is the reference mix which used 100% cement. CF and CS are two binary mixes in which cement is partially replaced by fly ash and silica fume, respectively. CFS is a ternary mix with the introduction of both of the SCMs. All the mixes were designed to have the same flowability in terms of flow diameter, which was tested by a small slump cone test. In addition, each mix was designed with a minimum w/b that can be obtained with the constituted materials. Therefore, the dosage of the superplasticiser was optimised for each mix through several trial mixes to satisfy the designed flowability and to find the limit to which the w/b ratio can be lowered. From Table 2, it can be seen that the introduction of the fly ash or silica fume reduced the water demand, which mainly results from an increased packing density by the SCMs. The addition of the fine SCMs can fill into the voids between the cement grains and thus free some extra water. This benefit was more pronounced for the ternary mix CFS as compared with the binary mixes because successive filling of the interstices between the cement grains by first the fly ash particles and then the silica fume particles can further increase the packing density. In addition, more superplasticiser was demanded for mixes CS and CFS because the specific surface area of the solid powders is significantly increased with the addition of silica fume.

A NJ-160 paste mixer with two different revolving speeds (140 and 285 r/min) and a mixing capacity of 1 l was used to prepare the pastes. For each mix, approximately 0·5 l paste was prepared in one batch, which was enough to prepare all the specimens. The dry materials were initially mixed at low speed for 2 min,

	Cement	Silica fume	Fly ash
Specific surface area: m^2/kg	362	22 200	454
Specific gravity	3·1	2·26	2·24
Silicon dioxide (SiO_2): %	21·35	91·2	54·11
Aluminium oxide (Al_2O_3): %	4·67	2·22	26·51
Iron (III) oxide (Fe_2O_3): %	3·31	0·88	6·40
Calcium oxide (CaO): %	62·6	1·2	4·70
Magnesium oxide (MgO): %	3·08	1·25	1·04
Sulfur trioxide (SO_3): %	2·25	0·64	1·29
Sodium oxide (Na_2O): %	0·54	—	2·22
Potassium oxide (K_2O): %	0·21	—	0·87
Loss on ignition (LOI): %	1·45	2·14	2·85

Table 1. Physical properties and chemical composition of cementitious materials

	Cementitious material: kg/m^3			Water to binder ratio[a]	Superplasticiser: % solid by mass of binder
	Cement	Fly ash	Silica fume		
C	1865	—	—	0·2	0·78
CF	1088	725	—	0·18	0·78
CS	1590	—	281	0·17	0·98
CFS	875	612	263	0·16	0·98

[a] Water in superplasticiser is included.

Table 2. Mix proportions

which helped break apart the agglomerates and homogenise the material. Then water and superplasticiser were added and the material was mixed at the high speed for 5 min to obtain good flowability. Afterwards, the paste was cast into a polyvinyl chloride tube with a diameter of 15 mm and a length of about 20 mm. Eight specimens were prepared for each mix, and the weight of a specimen was about 8 g. The specimens underwent standard moisture curing for 1 d at a controlled temperature of $20 \pm 2°C$ and relative humidity $> 95\%$ before they were demoulded and cured under two different regimes: one is the continued standard curing to prescribed ages (3, 7, 28 and 90 d), and the other one is steam curing in an enclosed steam chamber at 80°C for 2 d.

After the completion of prescribed curing, the specimens were soaked in ethanol for 7 d to terminate hydration. Then the specimens were oven-dried at 50°C for 2 d to remove the ethanol before testing.

Experimental programme

The pore structures of all the samples were studied by MIP using an Autopore 9500 instrument. MIP is based on the principle that a non-wetting liquid will only intrude into a porous medium under pressure. In this test, a sample was introduced into a chamber, and the chamber was evacuated before the sample was surrounded by mercury. Then the pressure was gradually increased and mercury was forced into the pores of the sample. Assuming a cylindrical pore shape, the relationship between the applied pressure P and the pore diameter d is described by the Washburn equation (Washburn, 1921)

$$d = -\frac{4\gamma \cos\theta}{P}$$

where γ is the surface tension of mercury and θ is the contact angle of mercury. The values of γ and θ in this research were assumed to be 0·485 N/m and 130°, respectively.

MIP tests were conducted on both the standard cured pastes and their steam cured counterparts. Only one specimen was tested for each mix with a specified curing. The maximum intrusion pressure generated for the 28 d and 90 d standard cured samples was 310 MPa, which corresponded to a minimum pore size of 4·0 nm, whereas for the other samples the maximum pressure used was 241 MPa, which determined a minimum pore size of 5·1 nm. The minimum pressure generated was 3·5 kPa, which corresponded to a pore size of 360 μm.

The microstructure was studied on selected samples by a FEI Quanta 3D FEG environmental scanning electron microscope (SEM). For preparing the sample, the cylindrical specimen was broken apart by a hammer and a small fractured piece was preserved. The contents of air voids and the morphologies of reaction products were examined.

Results and discussion

Standard curing

Cumulative porosity

The cumulative porosities of the four series of cement pastes at different curing ages are presented in Figure 1. It can be observed that the measured pores of all the samples were mainly composed of two types of pores. One was macro-pores with pore sizes ranging from several tens to hundreds of micrometres, and the other one was micro-pores with pore sizes below 50 nm. For the intermediate range between these two types of pores, there was hardly any increase of porosity with the increased pressure. The macro-pores could mainly result from the air voids which are either entrapped in the fresh mix or entrained by the superplasticiser, and the micro-pores should be attributed to the capillary and gel pores formed during hydration.

Comparing the cumulative porosity curves shown in Figure 1, it can be found that the contents of macro-pores in pastes CS and CFS were generally higher than those in pastes C and CF, which indicates that the addition of silica fume tends to increase the amounts of macro-pores in the paste. This could be related to an increased viscosity of the fresh pastes with the addition of silica fume (Allan and Kukacka, 1996; Gesoğlu *et al.*, 2009) because the air voids formed during mixing are more likely to be entrapped in a paste with high viscosity. Figure 2 shows SEM images of the four pastes after 28 d of curing, and it can be readily observed that the air voids contents were quite different for the four pastes. There were hardly any air voids present in the pure cement paste, and a few present in CF, but much higher volumes of air voids were observed in CS and CFS. Moreover, from Figure 1(d), it can be seen that for sample CFS there was a sharp jump of porosity with the pore size decreased from 3 to 2 μm, which can also be attributed to the presence of an internal air void. As reported by Moro and Böhni (2002), at lower pressures, the air voids near the sample surface have been filled by mercury, whereas the internal air voids are still empty. The internal air voids, which are filled at higher pressures, can be considered as ink-bottle pores with very narrow entrance pores compared to their own sizes, so they are misinterpreted as much finer pores by MIP test.

For readiness of comparison, the total porosity of the blended cement pastes at different curing ages is plotted in Figure 3. As the maximum intrusion pressure used for the 28 d and 90 d cured pastes was higher than that for the 3 d and 7 d cured pastes, pores smaller than 5·1 nm were not taken into account to calculate the total porosity in Figure 3. As a general trend, the total porosity for all the pastes decreased with the increased curing age owing to the continuous hydration of cement or the pozzolanic reaction of the SCMs. Moreover, it can be observed that, for all the pastes, the porosity decreased significantly before 7 d and thereafter the decrease of porosity slowed down. This is because the hydration of cement has been almost completed at the early age, which fills up most of the inter-particle spaces. For the pure cement paste,

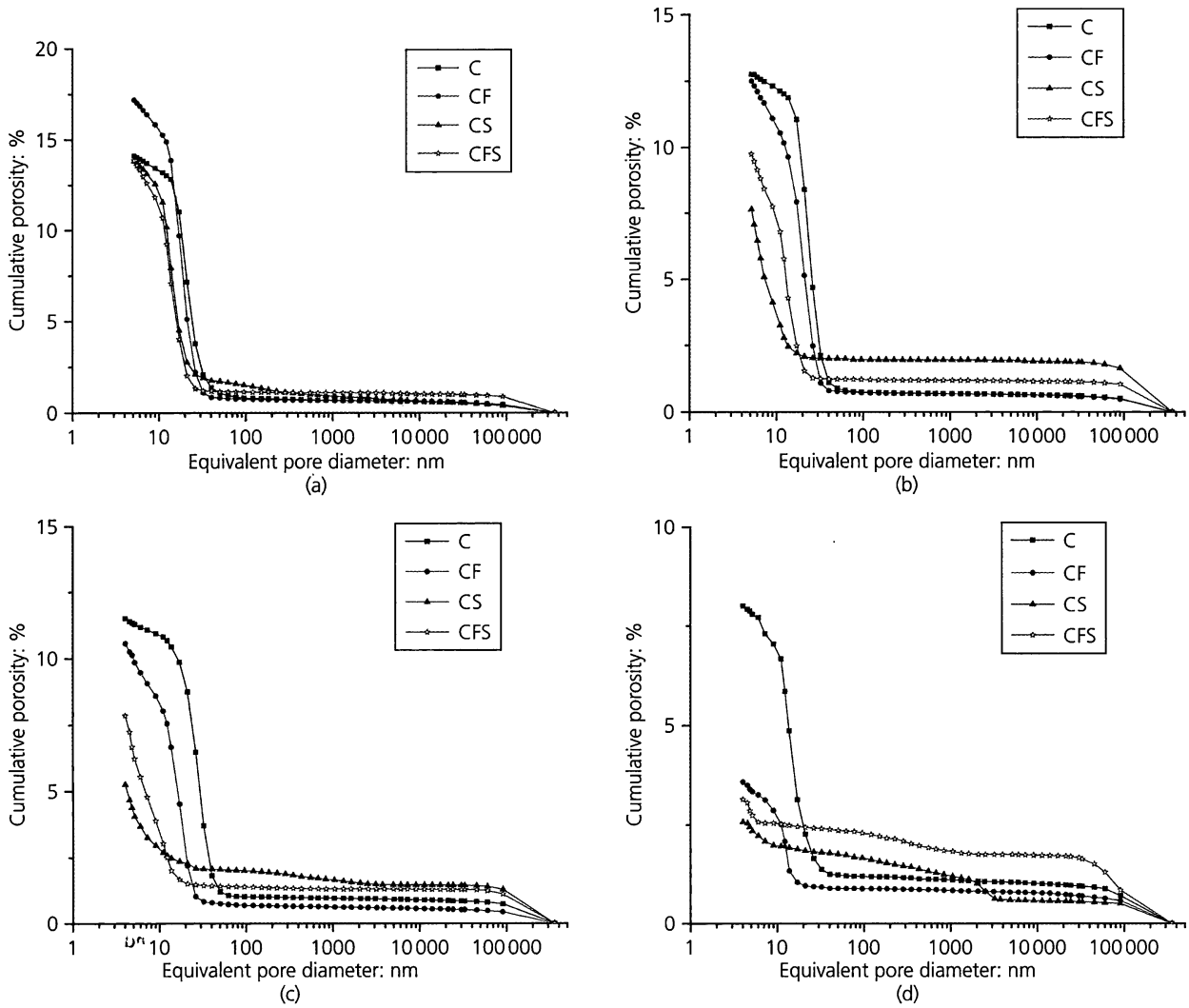

Figure 1. Cumulative porosity curves of four series of cement pastes at different curing ages: (a) 3 d; (b) 7 d; (c) 28 d; (d) 90 d

the porosity decreased from 14·1% at 3 d to 12·8% at 7 d. After 7 d, a thick layer of hydration products had already been formed around the unreacted clinker, which hindered the transport of reactants, so the porosity decreased almost linearly at a much lower rate. In addition, the deficiency of water and the restricted reaction space could also contribute to the slower reaction progress at the later age. For paste CF, the porosity decreased much faster from 3 to 7 d compared to the reference paste, which could be explained by the filler effect (Lothenbach *et al.*, 2011). Owing to its low reactivity, fly ash does not produce hydration products at the early age, so the effective water to cement (w/c) ratio is higher for the hydration of cement and thus more space is available for the hydration products of cement. After 7 d, with the start of the reaction between fly ash and calcium hydroxide (CH), more gel products are generated and thus the rate of decrease of porosity was still higher than that of the reference paste. For paste CS, the decrease of porosity was more pronounced from 3 to 7 d compared to the reference cement paste and CF. This is because silica fume has a relatively high pozzolanic activity, which causes the reaction between silica fume and calcium hydroxide to start as early as several hours after mixing (Poulsen *et al.*, 2009). Additional calcium silicate hydrate (C–S–H) with a decreased calcium/silicon (Ca/Si) ratio is formed and the volume of the calcium silicate hydrate gel is larger than the combined volume of calcium hydroxide and silica fume, so the capillary porosity is reduced and the paste becomes more compact. In addition, the smaller silica fume particles can provide extra surface to act as nucleation sites for the hydration products of cement, thereby accelerating the hydration of cement. From 7 to 28 d, the rate of decrease of porosity for CS was still higher than that for C, which indicates that the pozzolanic reaction is probably still ongoing during this period. At 28 d, the total porosity was very low (4·1%) and afterwards the porosity decreased slightly. For the ternary mix CFS, the decrease of

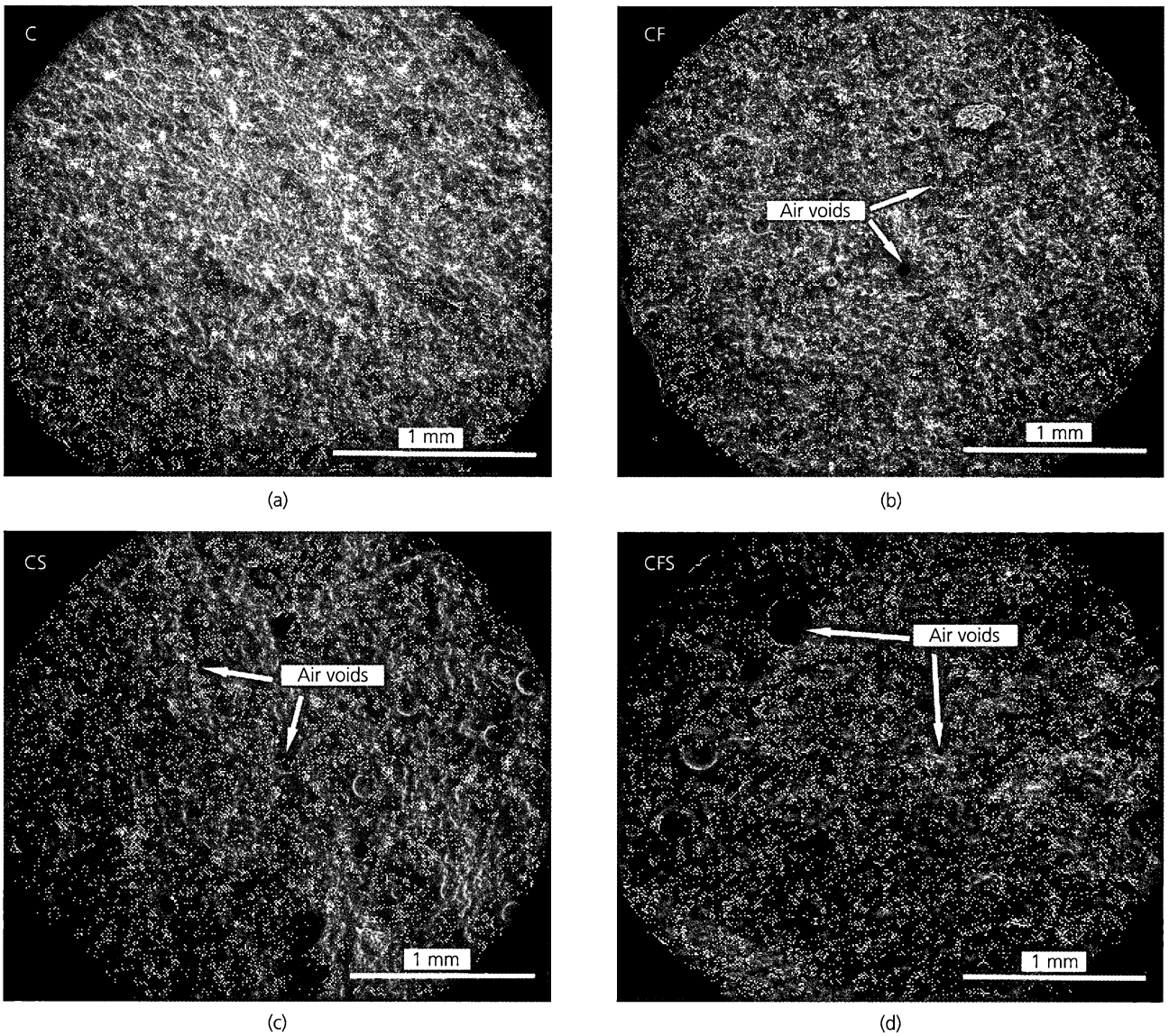

Figure 2. SEM images of the distribution of air voids in four series of cement pastes at the age of 28 d

porosity from 3 to 7 d was slower than that of CS but was comparable to that of CF. From 7 to 28 d, owing to the continuous pozzolanic reaction of silica fume, the reduced porosity content was similar to that of CS. However, after 28 d, the rate of decrease of porosity was higher than that of CS, which can be attributed to the reaction of fly ash. As most calcium hydroxide had been consumed by the reaction of silica fume and thus the pH of the pore solution decreased significantly, the reaction of fly ash in CFS was slower than that in CF.

The influence of the SCMs on the total porosity at all ages is also summarised in Figure 3. At 3 d, the porosity of CF was higher than that of the reference paste. This can be attributed to the lower cement content in CF, which creates fewer hydration products at the very early age. However, with the addition of silica fume, a slightly lower porosity than the reference paste was observed for CS and CFS. On one hand, the introduction of silica fume leads to a more compact packing and thus the space that needs to be filled by the reaction products is reduced. On the other hand, the pozzolanic reaction of silica fume in the first 3 d could generate considerable products to lower the porosity. Moreover, the nucleation effect provided by the small silica fume particles can accelerate the hydration of cement, which could also contribute to lowering the porosity at the very early age. At 7 d, with the porosity of CF being lower than C, all the blended pastes showed lower porosity than the reference paste from 7 to 90 d. CS had the lowest porosity throughout all of the curing ages, and the porosity of CFS was lower than CF but slightly

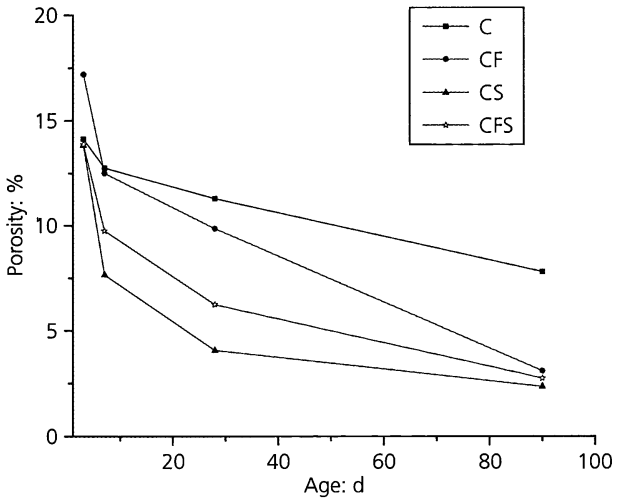

Figure 3. Summary of the effect of mix proportion and curing time on total porosity

higher than CS. At 90 d, the porosities of CF, CS and CFS were 3·1, 2·3 and 2·7%, respectively, which were very similar and much lower than the porosity of the reference paste (8·0%). This may indicate that the porosities of the blended pastes almost reach the minimum at 90 d. However, it should be noted that CS and CFS had much lower contents of micro-pores than CF because the volume of air voids accounts for the majority of the porosity in CS and CF at 90 d, which can be observed from the cumulative porosity curves.

From the results shown above, it can be concluded that the addition of silica fume significantly reduces the porosity and this effect is more prominent at the early age. The incorporation of fly ash slightly increases the porosity at the very early age, but after long-term curing, the porosity is much lower than the reference. Some studies (Yu and Ye, 2013; Zeng *et al.*, 2012) reported that for a paste with high volume of fly ash (30–60%) and a w/b ratio of 0·4 or 0·5, the porosity is always higher than the reference even after long-term curing, which is quite different from the present authors' findings with very low w/b ratio materials. For a paste with a very low w/b ratio, the mixing water is insufficient for a complete hydration of cement and there exists unhydrated cement after long-term curing, so a pure cement paste and a fly ash–cement binary paste would generate almost the same amounts of calcium-silicate-hydrate gels through the hydration of cement. Apart from the hydration of cement, the pozzolanic reaction of fly ash can provide additional gel products to further fill the pore space, which leads to a reduction of the total porosity for the binary mix. However, for a high w/b ratio paste, the internal water can fulfil a complete hydration of cement. Therefore, compared with the pure cement paste, the slow reaction of fly ash in the binary paste cannot generate enough gel products to take up the water spaces that should have been filled by the hydration products of the replaced cement. This may explain the discrepant effects of fly ash on the pore structures of pastes with quite varied w/b ratios.

Differential pore size distribution

The differential curve was obtained by differentiating the cumulative intrusion curve as shown in Figure 1. The differential curve is usually presented by the volume log diameter distribution; that is, a plot of $dV/d\log d$ against d. Some previous studies reported that in general two peaks, an initial peak and a rounded peak, could be observed for a cement paste in the differential curve, but only one peak may appear for a cement paste with a low w/c ratio (Cook and Hover, 1999). The initial peak refers to the critical pore size at which mercury has penetrated the interior of a sample. As discussed previously, MIP cannot provide a true PSD, but the critical pore size can be considered an indicator of material durability because it is closely related to permeability and diffusion characteristics of cementitious materials (Garboczi and Bentz, 1999).

The differential intrusion curves of the four series of cement pastes at different curing ages are presented in Figure 4. The plot in the range of macro-pores provided few useful data because the calculated size of the air void was significantly dependent on the location of the air void in the sample. In addition, the small peak at 2 μm in Figure 4(d) for CS was a reflection of the jump on Figure 1(d). Therefore, the plots in Figure 4 were mainly analysed in the range of the micro-pores. As a general trend, the critical pore size decreased with curing as the reaction products grew into the pore space. The critical pore size of the reference cement paste showed some fluctuations before 28 d, but it decreased from about 20 nm at the early age to 12 nm at 90 d. To some extent, this result is consistent with Cook and Hover's findings (Cook and Hover, 1999), which reported that for a cement paste with a low w/c ratio, the critical pore size became stable after hydration for 3 d. For the binary paste with fly ash, the critical pore size was constant at 17 nm from 3 to 28 d and then dropped to 12 nm at 90 d. The binary paste with silica fume had a slightly low critical pore size of 12 nm at 3 d and thereafter no peak was observed in the differential curves at later ages. The critical pore size of the ternary paste CFS was similar to that of CS at 3 d, and at 28 and 90 d, it decreased to less than 5 nm.

It can be concluded that the addition of silica fume decreases the critical pore size at all ages. This can be explained by the relatively high pozzolanic activity of silica fume. More gel products are created to fill the capillary pores and thus the pore structure is refined. Although the addition of fly ash significantly decreased the total porosity after long-term curing, it has very limited influence on the critical pore size. However, as the reaction of fly ash generates additional gel products, it can be observed from Figures 4(c) and 4(d) that the content of large micro-pores was reduced with the addition of fly ash. Moreover, assuming the gel pore size to be smaller than 10 nm, it can be seen that a connected network can be formed through capillary pores in C and CF, but in CS and CFS, the capillary pores cannot

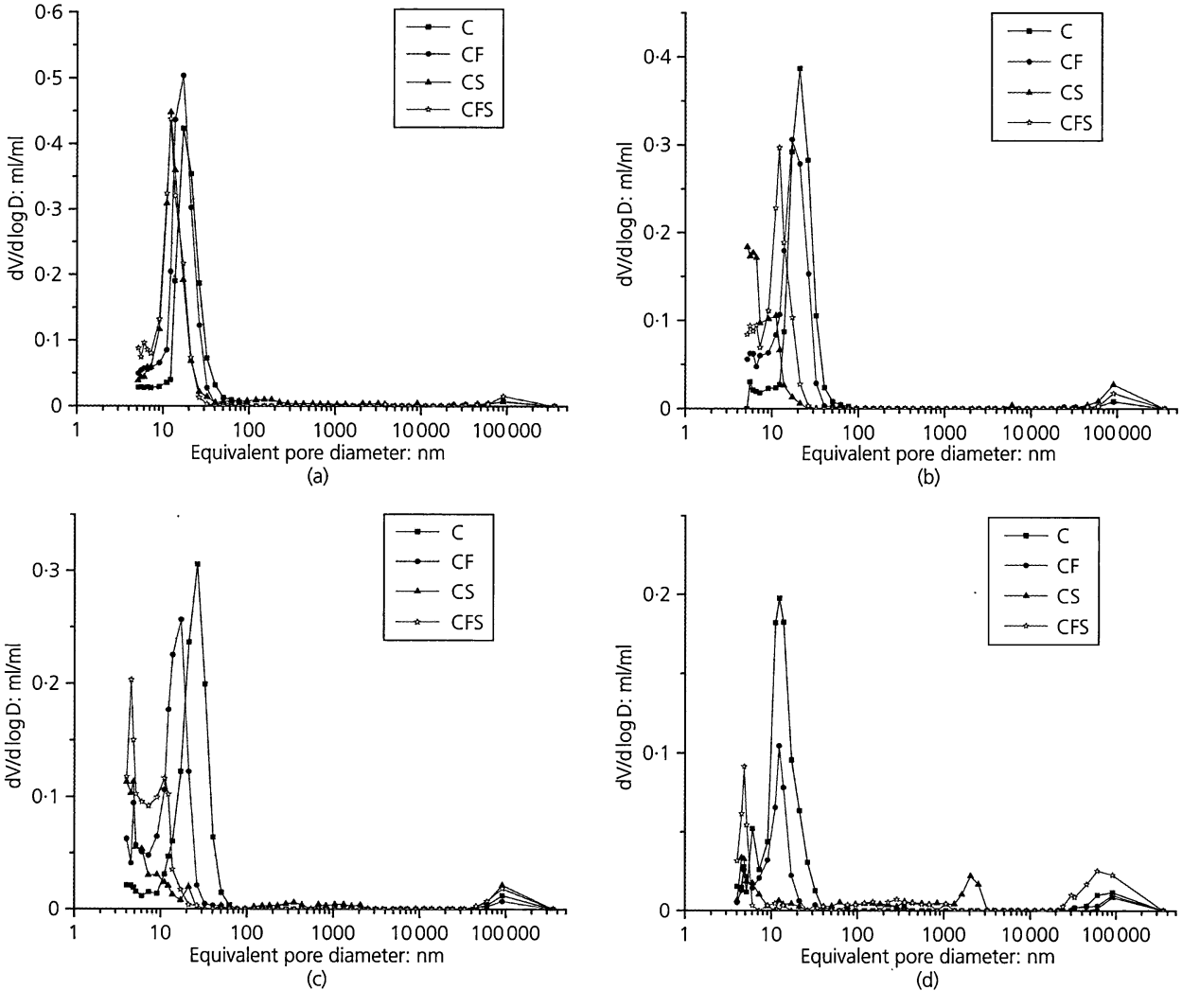

Figure 4. Differential pore size distribution curves of four series of cement pastes at different curing ages: (a) 3 d; (b) 7 d; (c) 28 d; (d) 90 d

percolate. Therefore, connected pathways in pastes CS and CFS should consist of disconnected capillary pores linked together by gel pores. As the transport of harmful liquids or gases is much faster in capillary pores than in gel pores (Garboczi and Bentz, 1992), the transport properties of CS and CFS should be dominated by the gel pores. Therefore, the pastes with silica fume could have a much higher durability than those without silica fume.

Bentz and Garboczi (1991) reported that the percolation threshold, a point at which the capillary pores no longer percolate, is 18% for the capillary porosity. If this is the case, for all the pastes in this study, a connected capillary pore system cannot be formed at all ages owing to their lower capillary porosities. This may imply that all the pastes have a very low permeability and diffusivity.

Steam curing

For low w/b ratio cementitious materials such as UHPC, one major application is steam-cured precast products such as plates and pipes. As the pozzolanic reactivity of SCMs significantly depends on the curing temperature (Hanehara *et al.*, 2001; Wild *et al.*, 1995), the influence of SCMs on the pore structures of steam cured pastes is studied.

The cumulative porosity and differential PSD curves of the four pastes after steam curing are given in Figure 5. It can be observed that all the pastes, especially the reference, showed lower total porosities than their 90 d standard cured counterparts. The total porosities of C, CF, CS and CFS after steam curing were 2·9, 2·1, 1·6 and 1·7%, respectively. The effects of the addition of silica fume or fly ash on the total porosity were similar to those observed on the 90 d standard cured samples.

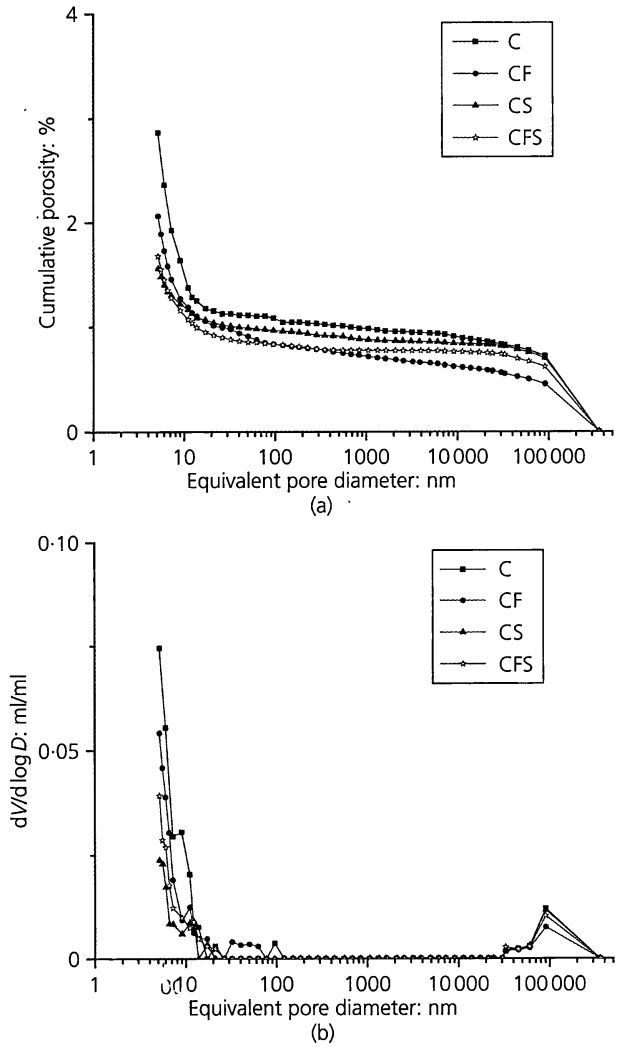

Figure 5. (a) Cumulative and (b) differential pore size distribution curves of four series of cement pastes after steam curing

In the differential curves, it is shown that no critical pore size was obtained, which indicates a very fine pore structure after steam curing. Furthermore, this may imply that the interior of the sample was not penetrated by mercury and thus the total porosity could be underestimated. The differential curves of the four pastes appeared quite similar, and compared with the results of the 90 d standard cured pastes, there was little change for CS and CFS, but the curves shifted toward smaller pore size for C and CF. This indicates that aging and heat treatment may have similar effects on the pore structure of CS and CFS, while for C and CF the pore structure is refined at the elevated temperature and probably more reaction products are formed. Figure 6 shows the micrograph of CF after steam curing, and it can be seen that the boundaries of the fly ash particles were blurred by amorphous gels, which may indicate the reaction of fly ash particles.

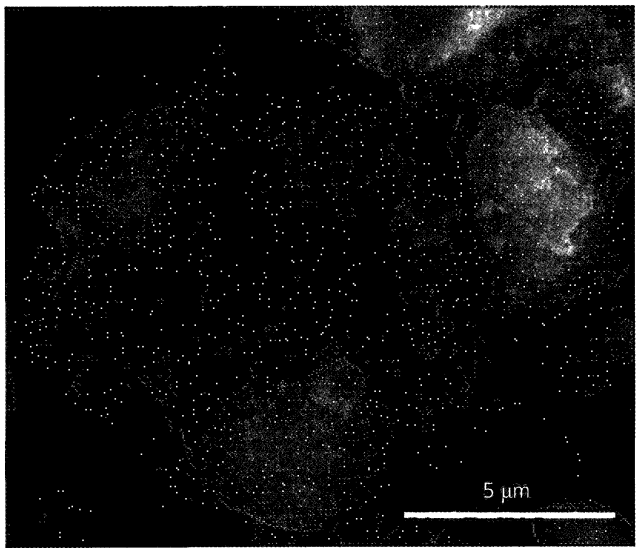

Figure 6. Microstructure of cement paste blended with fly ash after steam curing

Conclusions

This study investigated the influence of SCMs on the pore structures of blended pastes at very low w/b ratios. Besides the pure cement paste, two binary mixes and one ternary mix were prepared by introducing silica fume or fly ash. The samples were cured under two different regimes and their pore structures were tested by MIP.

The addition of silica fume significantly improved the pore structure under both standard moisture curing and steam curing. Although the addition of fly ash was reported to increase the total porosity for a cement paste with normal w/b, it was observed in this study to result in a decrease of porosity after 7 d for the low w/b paste. The critical pore size was almost unaffected with the addition of fly ash.

For preparing materials such as UHPC, silica fume is commonly used as an essential reactive powder. The findings from this study revealed that the pore structure of the ternary paste was similar to that of the silica fume binary paste after steam curing or long-term standard moisture curing, so it can be concluded that the addition of high volumes of fly ash does not harmfully affect the pore structures of materials like UHPC. The results could encourage the industry to produce these materials with partial replacement of cement by fly ash.

Acknowledgement

Financial support from National Basic Research Program of China (no. 2009CB623203) is gratefully acknowledged.

REFERENCES

Allan ML and Kukacka LE (1996) Comparison between slag-and silica fume-modified grouts. *ACI Materials Journal* **93(6)**: 559–568.

Atahan HN, Oktar ON and Taşdemir MA (2009) Effects of water-

cement ratio and curing time on the critical pore width of hardened cement paste. *Construction and Building Materials* **23(3)**: 1196–1200.

Bentz DP and Garboczi EJ (1991) Percolation of phases in a three-dimensional cement paste microstructural model. *Cement and Concrete Research* **21(2)**: 325–344.

Cheyrezy M, Maret V and Frouin L (1995) Microstructural analysis of RPC (reactive powder concrete). *Cement and Concrete Research* **25(7)**: 1491–1500.

Cook RA and Hover KC (1993) Mercury porosimetry of cement-based materials and associated correction factors. *ACI Materials Journal* **90(2)**: 152–161.

Cook RA and Hover KC (1999) Mercury porosimetry of hardened cement pastes. *Cement and Concrete Research* **29(6)**: 933–943.

Diamond S (2000) Mercury porosimetry: an inappropriate method for the measurement of pore size distributions in cement-based materials. *Cement and Concrete Research* **30(10)**: 1517–1525.

Garboczi EJ and Bentz DP (1992) Computer simulation of the diffusivity of cement-based materials. *Journal of Materials Science* **27(8)**: 2083–2092.

Garboczi EJ and Bentz DP (1999) Percolation aspects of cement paste and concrete-properties and durability. In *Proceedings of the American Concrete Institute Spring Convention*, vol. 189, pp. 147–164, Special Publication.

Gesoğlu M, Güneyisi E and Özbay E (2009) Properties of self-compacting concretes made with binary, ternary, and quaternary cementitious blends of fly ash, blast furnace slag, and silica fume. *Construction and Building Materials* **23(5)**: 1847–1854.

Hanehara S, Tomosawa F, Kobayakawa M *et al.* (2001) Effects of water/powder ratio, mixing ratio of fly ash, and curing temperature on pozzolanic reaction of fly ash in cement paste. *Cement and Concrete Research* **31(1)**: 31–39.

Lothenbach B, Scrivener K and Hooton RD (2011) Supplementary cementitious materials. *Cement and Concrete Research* **41(12)**: 1244–1256.

Mehta PK (2004) High-performance, high-volume fly ash concrete for sustainable development. In *Proceedings of the International Workshop on Sustainable Development and Concrete Technology* (Wang K (ed.)). Iowa State University, Ames, IA, USA, pp. 3–14.

Moro F and Böhni H (2002) Ink-bottle effect in mercury intrusion porosimetry of cement-based materials. *Journal of Colloid and Interface Science* **246(1)**: 135–149.

Poulsen SL, Jakobsen HJ and Skibsted J (2009) Methodologies for measuring the degree of reaction in Portland cement blends with supplementary cementitious materials by ^{27}Al and ^{29}Si MAS NMR spectroscopy. In *17. Internationale Baustoffiagung (ibausil)*. Bauhaus University, Weimar, Germany, pp. 177–188.

Radlinski M and Olek J (2012) Investigation into the synergistic effects in ternary cementitious systems containing Portland cement, fly ash and silica fume. *Cement and Concrete Composites* **34(4)**: 451–459.

Richard P and Cheyrezy M (1995) Composition of reactive powder concretes. *Cement and Concrete Research* **25(7)**: 1501–1511.

Scrivener KL (1989) The use of backscattered electron microscopy and image analysis to study the porosity of cement paste. In *Proceedings of Pore Structure and Permeability of Cementitious Materials* (Roberts LR and Skalny JP (eds)). Materials Research Society, Pittsburgh, PA, USA, vol. 137, pp. 129–140.

Seaton N (1991) Determination of the connectivity of porous solids from nitrogen sorption measurements. *Chemical Engineering Science* **46(8)**: 1895–1909.

Sun Z and Scherer GW (2010) Pore size and shape in mortar by thermoporometry. *Cement and Concrete Research* **40(5)**: 740–751.

Washburn EW (1921) Note on a method of determining the distribution of pore sizes in porous materials. *Proceedings of the National Academy of Sciences of the USA* **7(4)**: pp. 115–116.

Wild S, Sabir BB and Khatib JM (1995) Factors influencing strength development of concrete containing silica fume. *Cement and Concrete Research* **25(7)**: 1567–1580.

Yazıcı H, Yardımcı MY, Aydın S *et al.* (2009) Mechanical properties of reactive powder concrete containing mineral admixtures under different curing regimes. *Construction and Building Materials* **23(3)**: 1223–1231.

Yu Z and Ye G (2013) The pore structure of cement paste blended with fly ash. *Construction and Building Materials* **45**: 30–35.

Zeng Q, Li K, Fen-Chong T *et al.* (2012) Pore structure characterization of cement pastes blended with high-volume fly-ash. *Cement and Concrete Research* **42(1)**: 194–204.

Zhao S, Fan J and Sun W (2014) Utilization of iron ore tailings as fine aggregate in ultra-high performance concrete. *Construction and Building Materials* **50**: 540–548.

Zhou J, Ye G and Van Breugel K (2010) Characterization of pore structure in cement-based materials using pressurization–depressurization cycling mercury intrusion porosimetry (PDC-MIP). *Cement and Concrete Research* **40(7)**: 1120–1128.